# Numerical Investigation on Overlap Effects of Tandem Rotors in Forward Flight

**Jaewon Lee***
Research Institute of Mechanical Technology, Pusan National University, Busan, Korea

**Sejong Oh****
Department of Aerospace Engineering, Pusan National University, Busan, Korea

**Kwanjung Yee*****
Department of Aerospace Engineering, Pusan National University, Busan, Korea

**Deog-Kwan Kim******
Rotorcraft Program Office, Korea Aerospace Research Institute, Daejeon, Korea

## Abstract

A study on the interference effects of overlapping tandem rotors in forward flight is conducted using the time-marching free-wake panel method which adopts field velocity boundary integral formulation. The conventional boundary integral formulation is numerically unstable for the cases when the blade and the wake are in close proximity to each other. In order to avoid this problem, this study applies the field velocity method and modifies the boundary integration formulation. The improved method is used for the parametric study on the advance ratio and the distance between the rotors. These are the parameters that most affect the interference of the tandem rotor in forward flight. Comparison of the aerodynamic performance shows that the horizontal distance between the rotors negligibly influences the overlap-induced power factor for high advance ratio. In addition, it shows that the overlap-induced power factor is inversely proportional to the squared vertical distance between the rotors, and that the overlap-induced power factor increases to a certain extent and decrease back as the advance ratio increases.

Key words : Unsteady Panel Method, Time-Marching Free-Wake model, Rotor Overlap Effect, Field Velocity Approach

## Introduction

For the rotorcraft that generates lift, thrust, and control forces using rotating blades, the wake from the blades have serious effects on the aerodynamic characteristics of the aircraft and on the flow field around it. This means that it is critical for the analysis of the

* Researcher
** Professor
E-mail : tazo@pusan.ac.kr Tel : +82-51-510-2435 Fax : +82-51-513-3760
*** Associate Professor
**** Director

flight characteristics and the stability of the aircraft to accurately estimate the aerodynamic characteristics of the wake from the blade. Accurate estimation is especially critical for multi-rotor systems as a new extent for small vertical take-off and landing aircrafts. It is critical because the interference between the wakes from each rotor makes the aerodynamic characteristics remarkably more complex than that of a single-rotor system. The tandem rotor, one of the multi-rotor systems, has the rotor overlap effect that causes aerodynamic performance degradation, and its design and operation require profound understanding on the interference effects between the rotors.

There have been few experimental studies on aerodynamic characteristics of tandem rotors; Dingeldein[1] and Huston[2] in the 1950's and 1960's, and Stepniewski and Keys[3] in 1984. Stepniewski and Keys reviewed some experimental results, and used them to explain the interference effect based on the momentum theory. In addition, they use the experimental results to show that the interference effect of the front rotor on the induced power of the rear rotor is inversely proportional to the vertical distance between the front wake and the hub center of the rear rotor [3]. However, due to the limitations that the momentum theory has, the interference between wakes from adjacent rotors was ignored. Furthermore, the effect of individual design parameters, such as gap, stagger, and advance ratio, was not accounted for.

In terms of the numerical analysis, tandem rotors have an unsteady flow field and the effect of the wake is dominant even in hover. Therefore, the free-wake method and the potential method are often used, even in recent studies, because they represent the wake effects accurately with substantially less computational cost compared to computational fluid dynamics methods. Bagai and Leishman[4] used the free-wake method to estimate the wake trajectory of multi-rotor systems, including tandem configuration, and verified their analysis for coaxial rotors with the experimental results. Griffiths and Leishman[5] studied the interference of hovering tandem rotors. However, their research did not mention the cases of forward flight.

The authors of this paper have been studied aerodynamic problems of multi-rotor systems as a part of the development of a small multi-purpose multi-rotor unmanned aerial vehicle. The previous work [6] introduced an unsteady source-and-doublet panel code that adopts the time-marching free-wake approach which has small numerical diffusion and hence merits it in wake prediction. The code was used for the research on the effects of overlap of a hovering tandem rotor on the aerodynamic performance and for the prediction of the trajectory of the wake generated from a coaxial rotor [6].

The literature provides a physical and qualitative description of the overlap effects of tandem rotors. However, the substantial and quantitative understanding of how the design parameters affect the characteristics of the rotor-rotor interference on the tandem rotor in forward flight is still insufficient. This insufficiency is the major motivation for this study. This paper aims to conduct a detailed investigation into the effects of the design parameters of the tandem rotor – the gap, the stagger and the advance ratio – on the aerodynamic performance in forward flight and to provide guidelines on the design of overlap for the tandem rotor. This paper includes an investigational study into the variance of the interference in forward flight due to the changes in the overlapped area. This study is conducted by using an unsteady free-wake panel code which captures the interference of the wake well.

The doublet calculation using the standard boundary integral formulation has instability during the forward flight analysis of the tandem rotor when the blade panel is close to the wake. In order to resolve the issue of instability, this study uses the field velocity approach. In this approach, the vortex core model and vortex core growth model, which relax the instability on the wake trajectory, are also used for induced velocity calculation as well as velocity potential calculation. The modified approach is validated with the experimental results of Dingeldein's research [1]. In addition, the developed code is used for the parametric study on the variation of the design variables of the same configuration and thrust condition as used in Dingeldein's research. This code is also applied to the investigation into the effects of each parameter on the interference of the tandem rotors in forward flight.

# Numerical Analysis Method

## 2.1 The Unsteady Source-and-Doublet Panel Method

This study uses the unsteady source-and-doublet method, which is suitable for dealing with the effects from the thickness and complicated shapes of the blades. The panels are generated using the quadrilateral panel method which connects four points on the surface. Both the source and doublet strengths, $\sigma_\Phi$ and $\mu_\Phi$, are assumed to be uniform on each panel. In this case, the Dirichlet boundary condition for each of the N collocation points is as follows:

$$\sum_{K=1}^{N}\frac{1}{4\pi}\int_{\substack{body\\panel}}\mu_\Phi\hat{n}\cdot\nabla\left(\frac{1}{r}\right)ds+\sum_{K=1}^{N_w}\frac{1}{4\pi}\int_{\substack{wake\\panel}}\mu_\Phi\hat{n}\cdot\nabla\left(\frac{1}{r}\right)ds \\ -\sum_{K=1}^{N}\frac{1}{4\pi}\int_{\substack{body\\panel}}\sigma_\Phi\left(\frac{1}{r}\right)ds=0 \tag{1}$$

In order to enhance the efficiency of the calculations for induced velocity of the wake, its doublet panel is replaced by a rectangular vortex ring with the same potential strength. Next, the velocity induced by the vortex line is calculated using the Biot-Savart formula. In addition, Vatistas' vortex-core model [7] is used to resolve the singularity at the center of the vortex. The velocity at an arbitrary point in the flow field, which is induced by the vortex line as shown in Fig. 1, is calculated using the following equation:

$$\vec{V}=\frac{\Gamma}{4\pi}\frac{h}{\left(r_c^{2n}+h^{2n}\right)^{1/n}}\left(\cos\theta_1-\cos\theta_2\right)\hat{e} \tag{2}$$

In order to artificially add the viscous diffusion effect on the vortex, Squire's vortex-core growth model [8] is used as follows:

$$r_c(\zeta)=\sqrt{r_{c0}^2+4\alpha\delta\nu\zeta/\Omega} \tag{3}$$

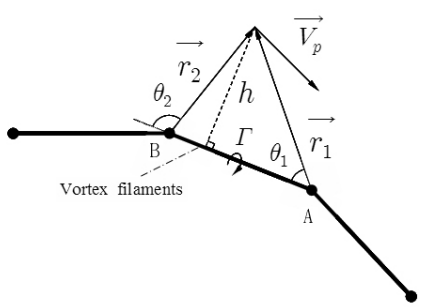


Fig. 1. Schematic of the induced velocity by a vortex line

where, $\alpha$ = 1.25643 is the Lamb-Oseen constant, and $\delta$ is the average effective viscosity coefficient. In this study, the initial radius of the vortex core is set to be 10% of the blade chord.

Following the Kutta condition, the doublet strength of the newest wake is set to be equal to the difference between the doublet strengths on the upper surface and lower surface of the trailing edge. The pressure coefficient is calculated using Bernoulli's equation, and it is corrected by Karman-Tsien's law [9] which uses nonlinear aspects of the flow.

## 2.2 The Field Velocity Approach

In general, in order to find the particular solution to Equation (1), the source distribution is determined using Equation (4), which is derived from Neumann's boundary condition. This means that the magnitude of the source is the same as the kinematic velocity at the collocation point.

$$\sigma_{\Phi} = -\hat{n} \cdot (\vec{V}_0 + \vec{v}_{rel} + \vec{\Omega} \times \vec{r}) \tag{4}$$

However, unlike the induced velocity in Equation (2), the velocity potential from Equations (1) and (4) does not reflect the vortex-core model and the vortex-core growth model. This difference implies that there is a discrepancy between the derivative of the velocity potential and the velocity. It is also observed that, if the vortex panel is close to the blade panel during the calculation process, instability appears in doublet of the blade panel. This causes an unstable trend, rather than a periodic, such as the dotted line shown in Fig. 2, at a flight condition, when the vortex collides with the blade surface.

In order to remove instability, the field velocity approach is applied to this study. The field velocity approach is a method used to bridge the wake models and the rotor wake in the flow field analysis using Euler or Navier-Stokes solvers. The computational fluid dynamics (CFD) solvers are used for air load analysis at the near field, while the free-wake method is used to account for the influence of the tip vortex. Here, the field velocity method applies the induced velocity generated by the tip vortex to the flow field of the CFD solver [10]. By applying the field velocity approach to the panel method, Gennaretti and Bernardini [11] divided the wake into two sub-wakes: the near wake and the far wake. They then replaced the influence of the far wake by the induced velocity, not by the potential integral. Their intention in doing this was to resolve the instability due to the blade-vortex interaction (BVI).

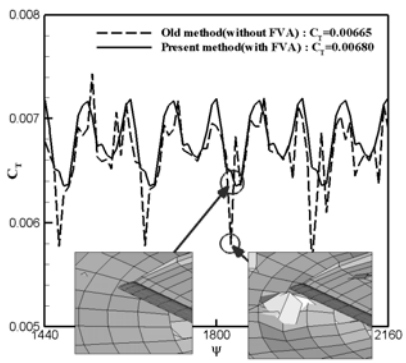


Fig. 2. Thrust coefficient history of tandem rotor with respect to analysis methods

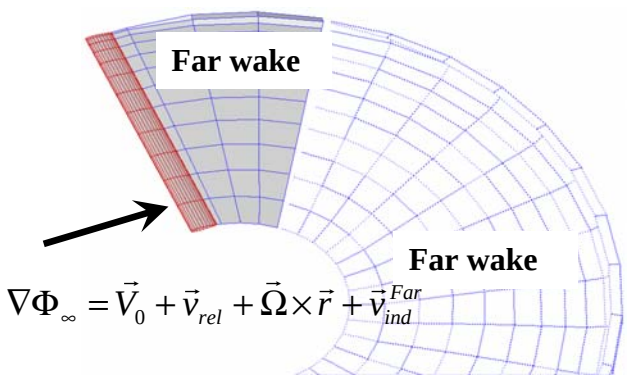


Fig. 3. Near wake and far wake

The near wake and far wake are designated as shown in Fig. 3. The induced velocity due to the far wake is replaced by the field velocity as in Equation (5). Next the Neumann boundary condition in Equation (4) is replaced by Equation (6). Furthermore, Equation (1) is rearranged into Equation (7).

$$\vec{v}_{ind}^{\,Far} = \sum_{K=1}^{N_w^{Far}} \frac{1}{4\pi} \int_{panel}^{wake} \mu_\Phi \nabla \left[ \frac{\partial}{\partial n} \left( \frac{1}{r} \right) \right] ds \tag{5}$$

$$\sigma_{\Phi,FVA} = -\hat{n} \cdot (\vec{V}_0 + \vec{v}_{rel} + \vec{\Omega} \times \vec{r} + \vec{v}_{ind}^{\,Far}) \tag{6}$$

$$\begin{aligned} &\sum_{K=1}^{N} \frac{1}{4\pi} \int_{panel}^{body} \mu_\Phi \hat{n} \cdot \nabla \left( \frac{1}{r} \right) ds + \sum_{K=1}^{N_w^{Near}} \frac{1}{4\pi} \int_{panel}^{wake} \mu_\Phi \hat{n} \cdot \nabla \left( \frac{1}{r} \right) ds \\ &- \sum_{K=1}^{N} \frac{1}{4\pi} \int_{panel}^{body} \sigma_{\Phi,FVA} \left( \frac{1}{r} \right) ds = 0 \end{aligned} \tag{7}$$

In this study, wake panels, whose wake age are equal to or less than 10° , are designated as the near wake part. The velocity potential, obtained from Equations (6) and (7), on the blade panel takes into account the vortex-core model and the influence of viscosity. The thrust coefficient, obtained from the modified equation, exhibits a periodic trend, shown as the solid line in Fig. 2. This trend is more physically feasible than the case without the field velocity approach.

### 2.3 Power Required

The total power required for a helicopter in forward flight is the sum of induced power, profile power, and parasite power. However, due to the lack of ability to account for the viscosity effect, potential-based approaches cannot directly estimate the profile power or parasite power. This study employs the table look-up which reads the drag coefficient at each airfoil section from the 2-D aerodynamic data table, and then calculates the profile power. The 2-D airfoil data is a C-81 format table that contains experimental values of lift, drag and pitching moment coefficients in terms of angle of attack, $\alpha$ , and Mach number, $M$ . In this study, the lift coefficient of each blade section is found using the panel method. Then the lift coefficient is used to determine the drag and pitching moment coefficients. The drag coefficient at each blade segment is calculated using the bilinear interpolation of the angles of attack and Mach numbers. Next, the drag is integrated along with the span to estimate the profile power.

The parasite power is power loss due to viscous shear effects and flow separation on the fuselage and rotor hub. It is a function of the reference area, $S_{ref}$ , multiplied by its drag coefficient , $C_{D_f}$ . The parasite power coefficient is calculated from Equation (8), where $A$ is the rotor disk area, and $f$ is the equivalent flat plate area.

$$C_{P_p} = \frac{1}{2} \left( \frac{S_{ref}}{A} \right) \mu^3 C_{D_f} = \frac{1}{2} \left( \frac{f}{A} \right) \mu^3 \tag{8}$$

## Analysis Results

### 3.1 Validation of the Tandem Rotor in Forward Flight

The aerodynamic performance analysis results from this study, for the tandem rotor in forward flight, were validated by Dingeldein's experimental results [1]. The tandem rotor

used in Dingeldein's experiment had two 2-rectangular-bladed rotors with a diameter of 4.572m and a NACA0012 airfoil without twist. The solidity of each rotor was 0.054. There was no gap between the rotor disks. Also the stagger was 3% of the rotor diameter. During his experiment, Dingeldein installed the front rotor first, trimming it at the fixed thrust coefficient of 0.0034, and then he added the rear rotor. He measured the power coefficient at the time when the thrust coefficient was doubled. He used the same setting as the single rotor test for the control input to the front rotor, while trimming the tandem rotor by controlling the rear rotor only. This study followed Dingeldein's procedure for the trim calculation. In order to account for the parasite drag due to the fuselage, the same equivalent flat plate area, which is 0.1858m2, was applied to the calculation. In order to make the thrust balance the parasite drag, the rotor tip path plane angle, $\alpha_{TPP}$, was determined by Equation (9). The set of $\alpha_{TPP}$ used in the analysis is shown in Table 1.

$$\alpha_{TPP} = \sin^{-1}\left(\frac{D_f}{T}\right) = \sin^{-1}\left(\frac{f\mu^2}{2C_T A}\right) \tag{9}$$

Fig. 4 exhibits the trim calculation results. It is observed that the rear rotor, which is influenced by the wake from the front rotor, has a relatively high collective pitch angle. Furthermore, the difference in the collective angle, between the rotors, decreased from about 1.9° at the advance ratio of 0.075, to 0.6° at the advance ratio of 0.295. This shows that the influence of the wake, from the front rotor on the rear rotor, is diminishing as the advance ratio increases. Further details on the variation in interference of the tandem rotors, according to the advance ratio, are discussed later.

Table 1. Rotor tip path plane angles

| Advance ratio | $\alpha_{TPP}$, ° |
|---|---|
| 0.075 | −0.27 |
| 0.110 | −0.58 |
| 0.145 | −1.00 |
| 0.190 | −1.72 |
| 0.240 | −2.75 |
| 0.295 | −4.15 |

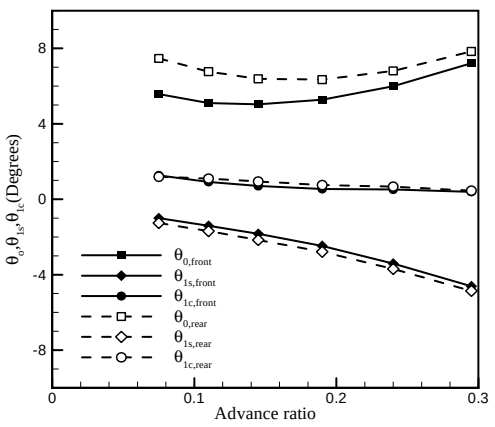


Fig. 4. Tandem rotor's control angles required for trim

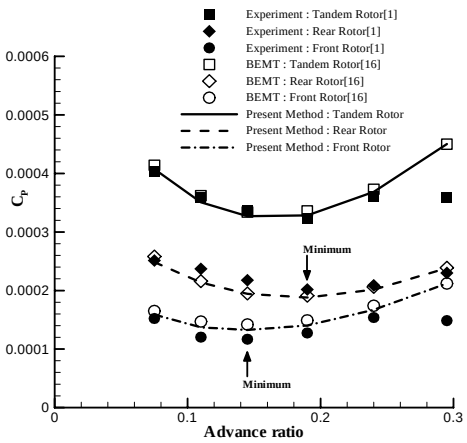


Fig. 5. Level-flight performance with tandem rotor

Fig. 5 shows the power required in terms of advance ratio. Since this study uses table look-up for the profile power calculation, the performance results are sensitive to the 2-D airfoil data in the table. The standard roughness 2-D airfoil aerodynamic data used in this study is from Ref. [12]. $C_{d_0}$ for this plot is 0.01. Leishman used this same $C_{d_0}$ to reproduce Dingeldein's experimental data by the analysis using the blade element momentum theory (BEMT).

Except for the case which has an advance ratio of 0.295, the general trend follows both the experimental data and BEMT results. Furthermore, the present approach correctly captures the trend, which the lowest power coefficient of the rear rotor appears at the higher advance ratio than that of the front rotor. Dingeldein remarked this trend as characteristic of tandem rotors. Both the present approach and the BEMT overestimate the power coefficient for the front rotor, while underestimating it for the rear rotor. However, the power coefficient of the tandem rotor, which is the sum of both estimations, correlates well with the experimental data.

### 3.2 Interference due to the Overlap

The influence of the overlap of the rotors in forward flight is investigated with the developed code. The rotor configuration, identical to that of Dingeldein's test, is used in the calculation. The definition of overlap area and the distance between the rotors are illustrated in Fig. 6.

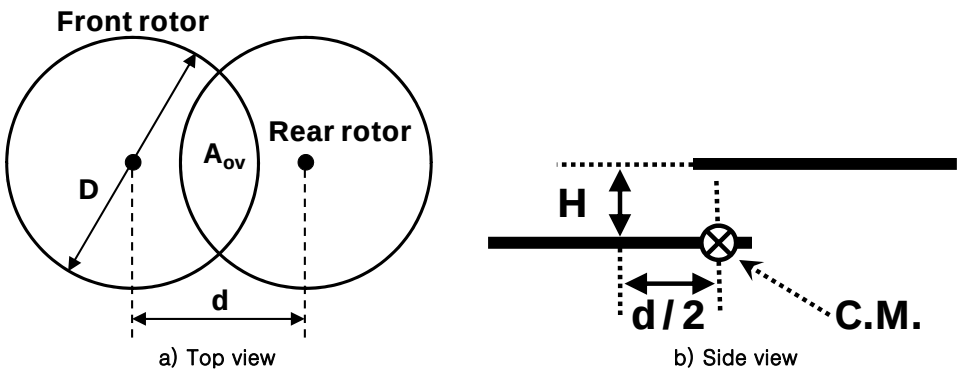


Fig. 6. Definitions of overlap area

The influence of the overlap on the inflow is investigated by looking into the variation of the induced power. The overlap induced power factor, $\kappa_{ov}$, is the ratio of the induced power of the overlapped rotors to the sum of the individual induced powers of the separate rotors, and is given in Equation (10).

$$\kappa_{ov} = \frac{(P_i)_{\text{tandem}}}{2(P_i)_{\text{single}}} \tag{10}$$

It is known, for hovering cases, from Ref. [6] that $\kappa_{ov}$ increases as d/D decreases and decreases as H/D increases, as shown in Fig. 7. It is also shown in the Fig. 7 that when the lower rotor is in the fully contracted wake of the upper rotor, the variance of $\kappa_{ov}$ also stabilizes. In other words, once the wake from the upper rotor is fully contracted, the area in which the wake affects the lower rotor does not vary along the distance, and hence the influence of H/D does not vary either.

In forward flight, the wake from the front rotor wraps all the way around the rear rotor disk and passes below it. Therefore, the rear rotor is influenced by the front rotor

more during forward flight than hover, while the rear rotor scarcely affects the front rotor. Fig. 8 shows the induced inflow distribution measured both over the single rotor disk and each rotor disk of the tandem rotors. It is observed that the inflow over the front rotor is similar to that of only a single rotor. However, the inflow over the rear rotor disk is increasing compared to the single rotor. Furthermore, Fig. 9 is the graph of the relationship between the induced power coefficient and the advance ratio, which shows that the single rotor and the front rotor of a tandem rotor have a similar induced power. Therefore, the conclusion can be drawn that the interference of the tandem rotor is proportional to the amount of the variation in the induced power of the rear rotor. Following the momentum theory, the interference from the wake of the front rotor, which influences the rear rotor, can be determined by a function of the vertical distance between the front wake and the center of the rear rotor hub, $h_{rr}$ [3]. $h_{rr}$ depends on the wake skew angle, $\chi$, and the distance between two rotors, d/D and H/D, while $\chi$ is found by the momentum theory as Equation (11) in terms of the advance ratio, $\mu$, and inflow of the front rotor. Fig. 10 illustrates the definitions of $\chi$ and $h_{rr}$.

$$\chi = \tan^{-1}\frac{\mu}{-\mu\sin\alpha_{TPP} + \lambda_i} \tag{11}$$

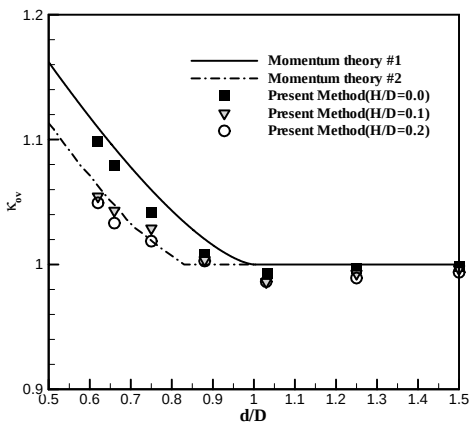


Fig. 7. Induced power factor vs. d/D: hovering mode

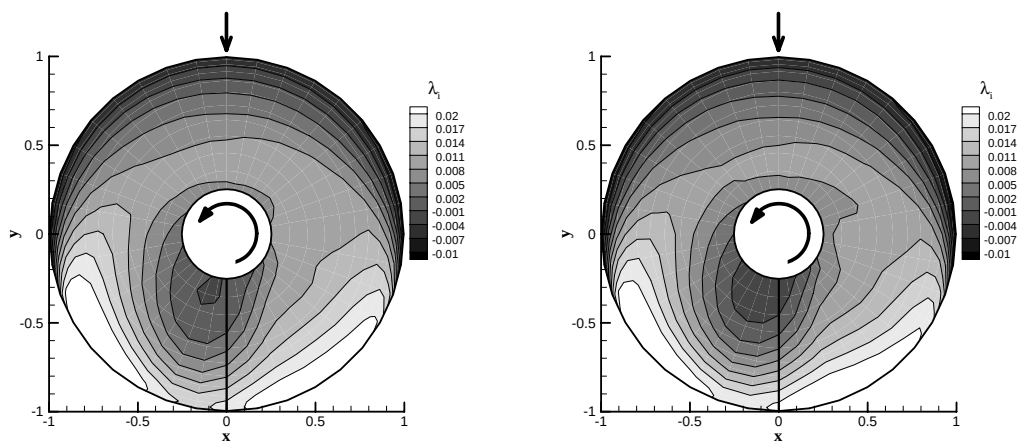


a) Single rotor b) Front rotor: d/D=0.7, H/D=0.2

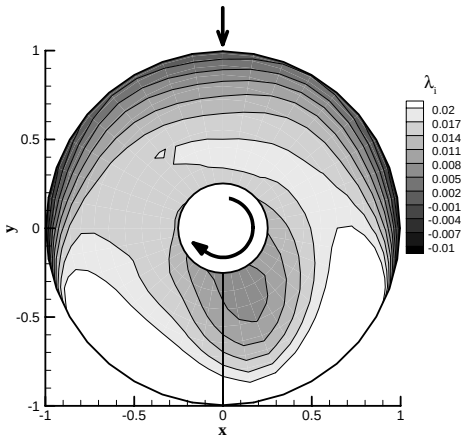


c) Rear rotor: d/D=0.7, H/D=0.2

Fig. 8. Induced inflow ratio of single rotor and tandem rotor($\mu$ =0.19)

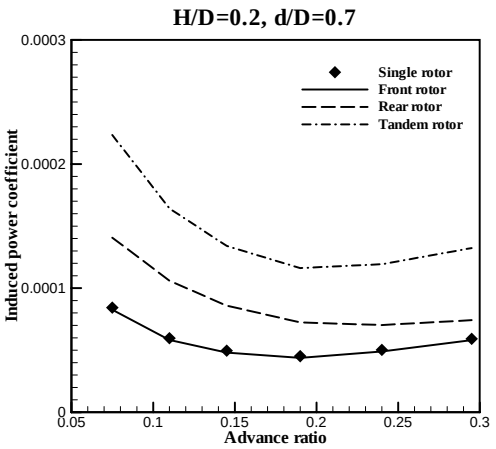


Fig. 9. Induced power coefficient vs. advance ratio

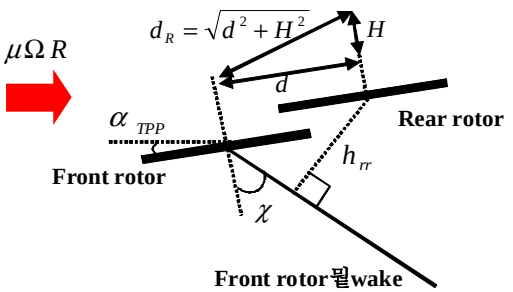


Fig. 10. Definitions of $\chi$ and $h_{rr}$

$$h_{rr} = \sqrt{d^2 + H^2}\sin\left(\frac{\pi}{2} - \chi + \tan^{-1}\left(\frac{H}{D}\right)\right) \tag{12}$$

According to Ref. [3], $h_{rr}$ can be calculated by Equation (12) based on the momentum theory. In addition, the experimental results exhibit that $\kappa_{ov}$ is inversely proportional to $h_{rr}$, and $\kappa_{ov}$ has its maximum value of 2.11 for $h_{rr}$ of 0. However, the tests were conducted by changing the thrust of the front rotor, $\alpha_{TPP}$, and forward flight speed to measure $\kappa_{ov}$ depending on $h_{rr}$. Therefore, the study on the influence of the individual parameters on the interference of rotors at the same thrust is insufficient. In light of this, the present study conducted parametric analysis on $\kappa_{ov}$ for the stagger ($0.6 \leq d/D \leq 1.0$), the gap ($0.0 \leq H/D \leq 2.4$), and the advance ratio ($0.075 \leq \mu \leq 0.3$) at the same thrust condition as Dingeldein's test, and compared the characteristics of the interference depending on the overlap.

### 3.3 The Influence of the Stagger

Following the momentum theory, the induced inflow ratio, $\lambda_i$, over the rotor disk in forward flight is calculated as Equation (13). $\chi$ from Equation (11) using Equation (13) are shown in Table 2 for several advance ratios.

$$\lambda_i = \sqrt{\frac{\sqrt{\mu^4 + C_T^2} - \mu^2}{2}} \tag{13}$$

According to Equation (12), if the advance ratio and H/D are fixed, the only parameter that affects $h_{rr}$ is d/D. As d/D increases, $h_{rr}$ increases as well, while, according to Ref. [3], $\kappa_{ov}$ decreases. This is because, as Equation (2) exhibits, the induced velocity generated by the vortex line of the wake is inversely proportional to the gap squared.

Fig. 11 shows the analytical result of $\kappa_{ov}$ in terms of d/D at various combinations of advance ratio and H/D. For the advance ratio of 0.075, $\kappa_{ov}$ decreases as d/D increases. The decrease in $\kappa_{ov}$ is a consequence of the increment in $h_{rr}$ due to greater d/D.

However, for the advance ratio of 0.19, except for the small fluctuation at H/D=0.0, the variance of $\kappa_{ov}$ is less than 1% revealing that there is almost no influence of d/D. The reason for this is as follows: In the momentum theory, which assumes that the induced velocity is uniform over the rotor disk, $\lambda_i$ of the front rotor calculated by Equation (13) is about 0.0178 at the advance ratio of 0.19. However, as found from the distribution of $\lambda_i$ shown in Fig. 8(b), its value obtained by the free-wake model in this study is less than 0.0178 at most of the region. Ref. [13] also confirms, by comparing various inflow models and experimental results, that the uniform inflow model overestimates $\lambda_i$ over the free-wake or experimental results in forward flight. Therefore, it is reasonable to find smaller $\lambda_i$ from the estimation by the free-wake model than by Equation (13). Equation (11) implies that a smaller $\lambda_i$ results in a greater $\chi$. In other words, for $\mu$ greater than 0.19, $\chi$ from the free-wake model becomes greater than 82.94° , approaching 90° . When $\chi$ is close enough to 90° , Equation (12) is rearranged as follows, revealing that $h_{rr}$ is influenced only by H/D and that $\kappa_{ov}$ is not influenced by d/D at high advance ratio:

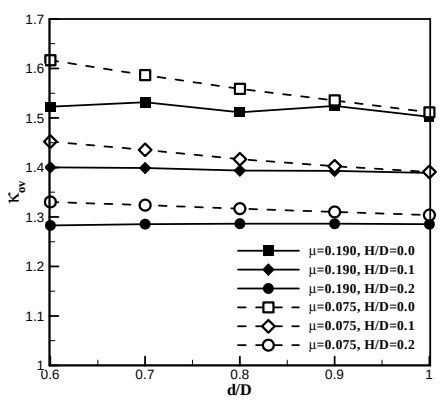


Fig. 11. Overlap induced power factor vs. d/D: forward flight mode

Table 2. Wake skew angles

| Advance ratio | $\chi$ , ° |
|---|---|
| 0.075 | 61.72 |
| 0.110 | 74.29 |
| 0.145 | 79.95 |
| 0.190 | 82.94 |
| 0.240 | 83.90 |
| 0.295 | 83.64 |

$$h_{rr} = \sqrt{d^2 + H^2}\sin\left(\tan^{-1}\left(\frac{H}{D}\right)\right)$$
$$= \sqrt{d^2 + H^2}\frac{H}{\sqrt{d^2 + H^2}} = H \quad (14)$$

In summary of the findings above, d/D and $\kappa_{ov}$ are inversely proportional to each other up to advance ratio = 0.19 and their relationship disappears beyond that point. The reason for this lies in the rise of $\lambda_i$ due to the higher advance ratio and its consequence on the high wake skew angle.The influence of the overlap of the rotors in forward flight is investigated with the developed code. The rotor configuration, identical to that of Dingeldein's test, is used in the calculation. The definition of overlap area and the distance between the rotors are illustrated in Fig. 6.

### 3.4 The Influence of the Gap

Since the velocity induced by the vortex line on an arbitrary point is inversely proportional to the gap squared as shown in Equation (2), if d/D and the advance ratio are fixed and the wake is assumed to be uniform as the momentum theory, one can see that the induced velocity is inversely proportional to H/D squared. Equation (15) is an approximation of the influence in terms of H/D based on the assumption above at d/D=0.7, where $a$ is a coefficient depending on the advance ratio.

$$\kappa_{ov} = \frac{a}{(H/D)^2 + 0.068} + 1.03 \quad (15)$$

Fig. 12 exhibits the analytic results of $\kappa_{ov}$ in terms of H/D for d/D of 0.7 at various advance ratios and the approximation by Equation (15). The general trend that $\kappa_{ov}$ inversely proportional to H/D squared is clearly noticeable in the figure.

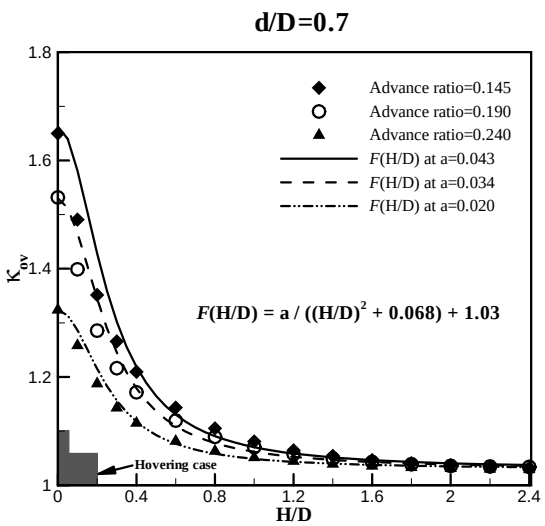


Fig. 12. Overlap induced power factor vs. H/D: forward flight mode

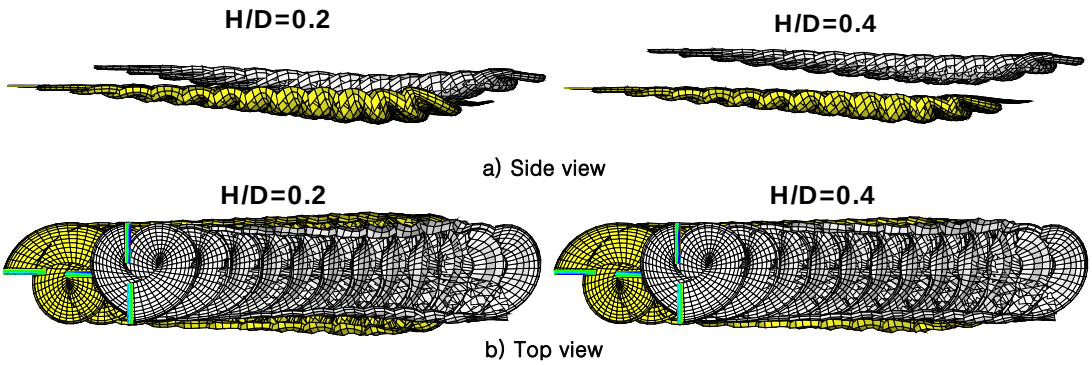


Fig. 13. Wake predictions for tandem rotors at various H/D( $\mu$ =0.19, d/D=0.7)

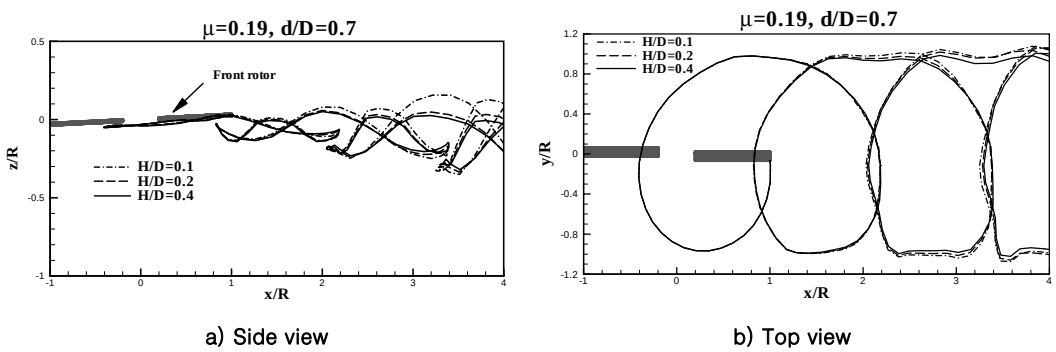


a) Side view b) Top view

Fig. 14. Tip vortex trajectories of front rotor at various H/D( $\psi$ =0° )

As H/D decreases, the wakes from the front rotor and the rear rotor get closer to each other increasing the wake-wake interaction. As a consequence, the wake is distorted more as H/D decreases. For two different H/D settings of 0.2 and 0.4, Fig. 13 shows the trajectory of the wake from the tandem rotor for d/D of 0.7 at the advance ratio of 0.19. For the small H/D, the wake from the front rotor expands wider and wraps around the wake from the rear rotor. The same influence of H/D on the trajectory of the wake from the front rotor can be observed in more detail from Fig. 14. It is clearly shown in Fig. 14 that, for the smaller H/D, the y/R trajectory of the blade tip vortex widens and z/R trajectory fluctuates more up and down.

## 3.5 The Influence of the Forward Speed

The analytical results of $\kappa_{ov}$ in terms of advance ratio for the fixed rotor distances are shown in Fig. 15. From the figure, it is observed that $\kappa_{ov}$ increases along with the advance ratio up to certain point and decrease back beyond that point. Independent of H/D, $\kappa_{ov}$ reaches the maximum at around $\mu$ =0.1 where, in general, is the boundary of high advance ratio for a rotorcraft.

This trend of $\kappa_{ov}$ can be discussed in two ways. $\kappa_{ov}$ indicates the variance of induced inflow over the rear rotor due to the wake from the front rotor, and the variance is determined by $h_{rr}$ and the density of the blade tip vortex line that passes under the rear rotor disk. According to Equation (12), for the fixed distance between the rotors, $h_{rr}$ is a function of $\chi$ only, and $\chi$ increases and $h_{rr}$ decreases for the increasing advance ratio.

The relation between $h_{rr}$ from Equation (12) and $\mu$ is shown in Fig. 16 for various H/D with d/D=0.7. Furthermore, as shown in Fig. 17, the blade tip vortex lines under the rear rotor disk gets sparser for higher advance ratio.

If $\mu$ is less than 0.11, besides the decreasing vortex line density, large drop of $h_{rr}$ dominates the rise of $\kappa_{ov}$ as shown in Fig. 15. Beyond 0.11, however, $h_{rr}$ settles as shown in Fig. 16, and hence the decreasing density of the vortex lines dominates the influence. As a consequence, $\kappa_{ov}$ decreases for $\mu$ >0.11.Since the velocity induced by the vortex line on an arbitrary point is inversely proportional to the gap squared as shown in Equation (2), if d/D and the advance ratio are fixed and the wake is assumed to be uniform as the momentum theory, one can see that the induced velocity is inversely proportional to H/D squared. Equation (15) is an approximation of the influence in terms of H/D based on the assumption above at d/D=0.7, where $a$ is a coefficient depending on the advance ratio.

## Conclusions

This study conducted a parametric analysis on the design parameters to investigate the influence of the overlap of tandem rotors on the forward flight performance. In the course of the forward flight analysis for the tandem rotor, the existing time-marching free-wake panel code presented instabilities on the magnitude of the potential for the cases that the blade and the wake are very close to each other. In order to resolve the instability, the field velocity approach was employed. The new code was validated with Dingeldein's test results, and then used for the analysis on the influence of each design parameter on the aerodynamic performance of the tandem rotors in forward flight. The interference of the tandem rotor was compared in terms of $\kappa_{ov}$ as follows:

Select Until certain value of $\mu$, d/D and $\kappa_{ov}$ were inversely proportional. However, beyond that value of $\mu$, d/D scarcely affects $\kappa_{ov}$.

$\kappa_{ov}$ was generally proportional to H/D squared. Furthermore, a relational formula between $\kappa_{ov}$ and H/D was drawn. It is found that, as H/D decreased, the y/R trajectory of the tip vortex from the front rotor widened and z/R trajectory fluctuated up and down more widely.

As the forward speed increased, $\kappa_{ov}$ rose and dropped back with its maximum at $\mu$ of 0.11.

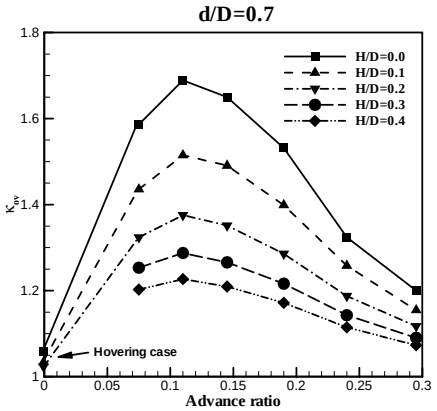


Fig. 15. Overlap induced power factor vs. advance ratio at various H/D

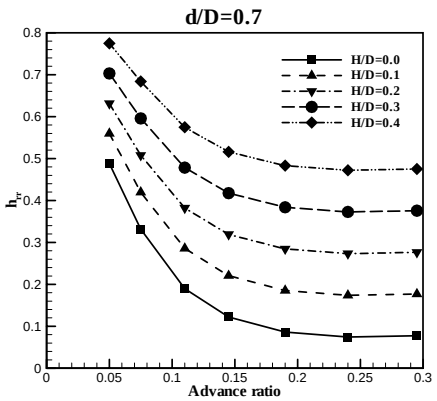


Fig. 16. $h_{rr}$ vs. $\mu$ at various H/D

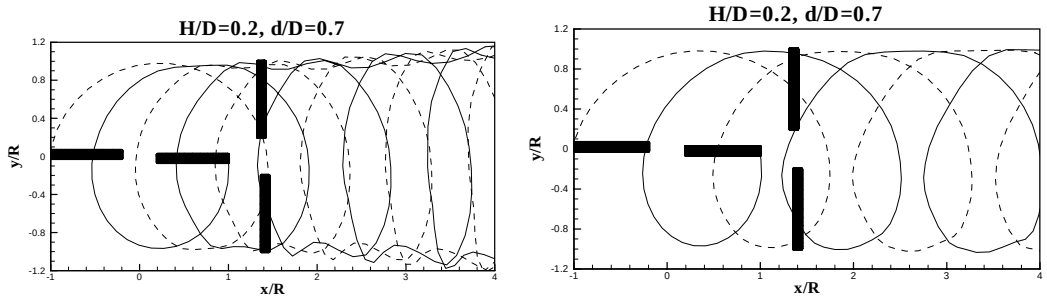


a) Advance ratio=0.145 b) Advance ratio=0.240

Fig. 17. Tip vortex trajectories of front rotor at various advance ratio

## Acknowledgments

This study has been supported by the KARI under KHP Dual-Use Component Development Program funded by the Ministry of Knowledge.

## References

1. Dingeldein, R. C., "Wind-tunnel Studies of the Performance of Multirotor Configurations," NACA TN 3236, 1954.

2. Huston, R. J., "Wind-tunnel Measurements of Performance, Blade Motions, and Blade Air Loads for Tandem-Rotor Configurations With and Without Overlap," NASA TN D-1971, 1963.

3. Stepniewski, W. Z., and Keys, C. N., Rotary-Wing Aerodynamics, Dover, New York, 1984, pp. 188-190.

4. Bagai, A., and Leishman, J. G., "Free-Wake Analysis of Tandem, Tilt-Rotor and Coaxial Rotor Configurations," Journal of the American Helicopter Society, Vol. 41, No.3, 1996, pp. 196-207.

5. Griffiths, D. A., and Leishman, J. G., "A Study of Dual-Rotor Interference and Ground Effect Using a Free-Vortex Wake Model", American Helicopter Society 58th Annual Forum [CD-ROM], Montreal, Canada, June 11-13, 2002.

6. Lee, J., Yee, K., and Oh, S., "Numerical Investigation of Dual Rotors Using a Time-Marching Free-Wake Method," American Helicopter Society 64th Annual Forum [CD-ROM], Montréal, Canada, April 29 May 1, 2008.

7. Vatistas, G. H., Kozel, V., and Mih, W., "A Simpler Model for Concentrated Vortices," Experiments in Fluids, Vol. 11, 1991, pp. 73-76.

8. Squire, H. B., "The Growth of a Vortex in Turbulent Flow", Aeronautical Quarterly, Vol. 16, Aug. 1965, pp. 302-306.

9. Anderson, J. D., Modern Compressible Flow with Historical Perspective, 3rd ed., McGraw Hill, New York, 2003, pp. 324-335.

10. Datta, A., Sitaraman, J., Baeder, J. D., and Chopra, I., "Analysis Refinements for Prediction of Rotor vibratory Loads in High-Speed Forward Flight", American Helicopter Society 60th Annual Forum [CD-ROM], Baltimore, MD, June 7~10, 2004.

11. Gennaretti, M., and Bernardini, G., "Novel Boundary Integral Formulation for Blade-Vortex Interaction Aerodynamics of Helicopter Rotors," AIAA Journal, Vol. 45, No. 6, 2007, pp. 1169-1176.

12. Abbott, I. H., and Doenhoff, A. E. V., Theory of Wing Sections Including a Summary of Airfoil Data, Dover, New York, 1959, pp. 462, 463.

13. Leishman, J. G., Principles of Helicopter Aerodynamics, 2nd ed., Cambridge University Press, New York, 2006, pp. 158-166.